A Comparison of Low- and High-Fidelity Models for Tail Rotor Icing Phenomena

Aishwerya Gahlot, Georgia Institute of Technology, Atlanta, GA, USA
Jeewoong Kim, Sikorsky, A Lockheed Martin Company, Stratford, CT, USA
Lakshmi N. Sankar, Georgia Institute of Technology, Atlanta, GA, USA

Abstract

A low-fidelity model for modeling ice accretion phenomena over two-bladed teetering rotors has been developed. In this approach, the blades are assumed to be rigid, and the flapping motion is caused by the inertial, centrifugal, and aerodynamic forces acting on the blade section. The aerodynamic forces are computed using a table look-up of precomputed airfoil lift and drag coefficients as a function of effective angle of attack. Following the analysis of the rotor without icing effects, ice shapes at selected radial locations on the rotor are computed. The impact of ice shapes on the 2-D lift and drag characteristics is estimated using a 2-D CFD analysis. Finally, the rotor is reanalyzed using the low fidelity model with the iced airfoil lift and drag characteristics. Calculations have been done for the dry rotor, and two specific icing test conditions. Comparisons with test data and a higher fidelity model are presented.

1. INTRODUCTION

The impact of icing on helicopter performance, handling qualities, safety, and availability are important considerations in rotorcraft design and development, particularly for helicopters and eVTOL configurations designed for cold weather operations. Considerable progress has been made over the past several decades in modeling ice accretion and deicing over 2-D and 3-D configurations [1- 4], and these tools are being used in combination with 3-D computational fluid dynamics analyses in fixed and rotary wing aircraft industries. Encouraging preliminary results have been obtained for rotor and propeller ice accretion phenomena [5-7]. There remains a need during the preliminary design stage for simpler low fidelity tools that can rapidly estimate the ice thickness and the impact on rotor performance for a variety of conditions.

2. SCOPE OF THE PRESENT WORK

In this study, a low-fidelity model with significantly lower computational cost has been formulated for modeling rotor icing. The entire process may be automated, where the individual tools for modeling this complex phenomenon are sequentially invoked. Encouraging preliminary results have been obtained for the ice accretion phenomena, for a two-bladed teetering tail rotor that was tested at NASA Glenn Research Center [7].

3. DESCRIPTION OF THE ROTOR TEST DATA

A detailed set of test data have been obtained at the NASA Glenn Research Center for a two-bladed teetering tail rotor under a Vertical Lift Consortium project with NASA, Boeing, Sikorsky, Bell, and Georgia Tech as partners [7, 8]. The blade planform is rectangular, with a radius of 32.6" and a chord length of 5.3". The blades are untwisted and made of NACA 0012 airfoil profiles. The blade profiles used in the test data are somewhat different, however, because of the addition of a heater blanket in the rotor leading edge region. The collective pitch angle, rotor RPM and the tunnel velocity may all be varied independently.

Available data include measured ice shapes, and the hub loads – specifically rotor thrust and torque under icing and deicing conditions.

Copyright Statement

The authors confirm that they, and/or their company or organization, hold copyright on all of the original material included in this paper. The authors also confirm that they have obtained permission, from the copyright holder of any third-party material included in this paper, to publish it as part of their paper. The authors confirm that they give permission or have obtained permission from the copyright holder of this paper, for the publication and distribution of this paper as part of the ERF proceedings or as individual offprints from the proceedings and for inclusion in a freely accessible web-based repository.

3. DESCRIPTION OF THE EXISTING HIGH-FIDELITY MODEL

Figure 1 shows the process that is used for modeling helicopter icing phenomenon using a high-fidelity model developed by the present authors [9].

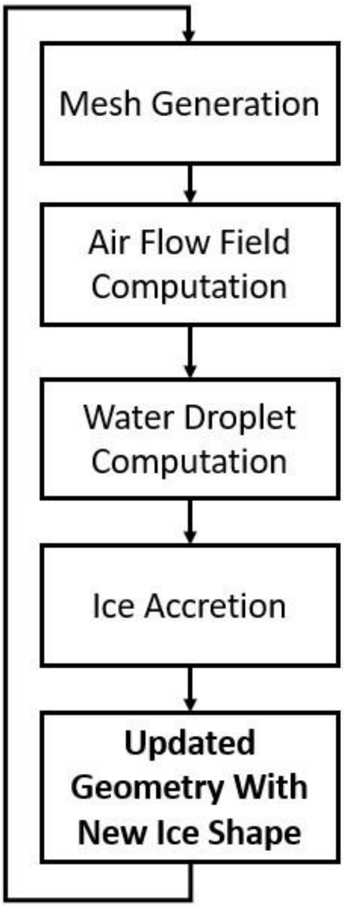

Figure 1: Overview of the High-Fidelity Model

An in-house C-H mesh generator was used to generate the body-fitted grid. The user has some control over the normal spacing so that the viscous layer over the blades is sufficiently resolved. The grid may also be clustered in the leading edge, trailing edge, and tip regions.

A hybrid Navier-Stokes/free wake methodology called GT-Hybrid has been used to model the unsteady aerodynamic phenomena over the rotor [9]. The aerodynamic analysis is performed on a structured body-fitted grid surrounding the reference rotor blade. This grid captures only the near field variations of density, velocity, and pressure, and the vorticity field in the wake immediately behind the rotor blade as shown in Figure 2. At the downstream boundary, the wake field is converted into equivalent trailing and shed vortex filament structures. These vortex filaments are allowed to move away from the rotor due to the self-induced velocity of the rotor, and the oncoming freestream. The wake structures from neighboring blades are also similarly modeled. The effect of the wake that lies outside the computational domain is felt by the body-fitted grid as induced velocity field specified at the computational inflow boundaries.

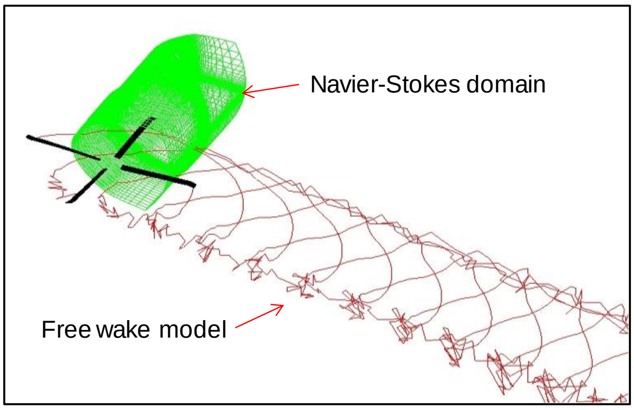

Figure 2: Overview of the Hybrid Navier-Stokes/Free Wake Methodology

A 3-D unsteady Eulerian transport model is subsequently used to model the transport of water droplets through the flow field and estimate the rate at which the water mass is deposited onto the blade surface. The following equations are solved using a finite volume scheme, on the same grid used by GT-Hybrid for computing the aerodynamics.

(1)
$$\frac{\partial}{\partial \tilde{t}} \iiint \alpha_w d\tilde{V} + \oiint \alpha_w \widetilde{\boldsymbol{V}_w} . d\widetilde{\boldsymbol{A}} = 0$$

(2)
$$\frac{\partial}{\partial \tilde{t}} \iiint \alpha_w \widetilde{\boldsymbol{V}_w} d\tilde{V} + \oiint (\alpha_w \widetilde{\boldsymbol{V}_w}) \widetilde{\boldsymbol{V}_w} . d\widetilde{\boldsymbol{A}} = \frac{\widetilde{\boldsymbol{F}}_{wa}^{drag} + \widetilde{\boldsymbol{F}}^{gravity} - \widetilde{\boldsymbol{F}}^{buoyant}}{\rho_w}$$

In this equation set, the unknowns are the volume fraction of water α_w and the water droplet velocity $\widetilde{\boldsymbol{V}_w}$. The right side of the second equation for the droplet velocity contains the Stokes drag force field experienced by the droplets as they move through the flow field, the effects of gravity, and buoyancy. The influence of the aerodynamic flow on the droplet transport enters into the formulation through the Stokes drag force term. Reference 9 gives full details of how these terms are computed.

A first order upwind scheme has been used to model the droplet flux entering and leaving the computational domain. An implicit time marching scheme is used, coupling the droplet volume fraction and droplet velocity field in each control volume with corresponding values in the neighbor cells leading to a sparse system of coupled equations. An LU approximate factorization scheme is used to invert the matrix and solve for the quantities of interest.

Mass balance and energy balance in the water layer are computed using an extended version of the Messinger model [11]. The energy balance requires the rate at which heat is transferred from the relatively warm water droplets to the cold rotor surface. Empirical heat transfer rates for laminar and turbulent flow are used, with the transition location determined using an empirical relationship that accounts for the roughness caused by the water droplets that freeze and form ice crystals. This formulation is documented in detail in Ref. 7.

Other ice accretion models such as the industry standard NASA Glenn LEWICE analysis may also be used. In such an approach, the surface pressure and the surface skin friction are specified from the CFD analysis. The normal component of the velocity of the water droplets in the vicinity of the rotor surface computed in the droplet transport solver, non-dimensionalized by the in-plane component velocity seen by the rotor blade section, is also specified.

Recently, the one-way coupling between the aerodynamic analysis and the droplet transport has been replaced with a fully coupled multi-species transport model [12].

4. DESCRIPTION OF THE BLADE DYNAMICS MODEL

The two-bladed teetering rotor is assumed to be rigid and allowed to freely flap up and down about a hinge at the center of the rotor disk, as shown in Figure 3 below. The blade dynamics should be defined with sufficient accuracy. This information is used to compute the velocity of the finite volume cell faces in aerodynamic analysis and the droplet transport solver.

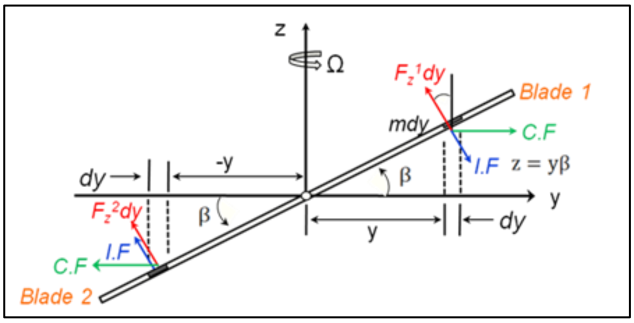

Figure 3: Freebody Diagram of the Teetering Rotor

At the central hinge, the moments caused by the aerodynamic, centrifugal and the inertial forces should add up to zero. The following equation is solved.

(3)

$$2I\left[\frac{d^2\beta}{dt^2}+\Omega^2\beta\right]=\int_{r=0}^{r=R}[F_{z1}-F_{z2}]rdr$$

In the above equation, the quantity I is the moment of inertia of an individual blade about the central hinge, Ω is the angular velocity of the rotor in radians per second, and β is the flapping angle. The quantities F_{z1} and F_{z2} are the aerodynamic forces per unit span, normal to the chord line at each section, located at the radial location r, on the first and second blades, respectively. In the high-fidelity approach, these forces were computed directly from the hybrid Navier Stokes/free wake flow solver.

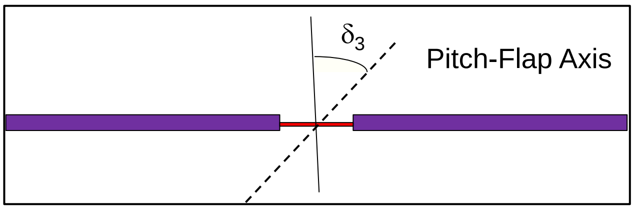

Figure 4: Pitch Flap Coupling

The blade pitching and flapping motion are coupled to each other, since the pitch-flap axis is inclined at an angle of δ_3 equal to 45 degrees for this rotor as shown in Figure 4. The following equation of motion may be written, linking the flapping motion $\beta(t)$ to the pitching motion $\theta(t)$.

(4)

$$\frac{d\beta}{dt}=-tan(\delta_3)\frac{d\theta}{dt}$$

The aerodynamics is coupled to the rotor flapping and pitching dynamics, and vice versa. A loosely coupled analysis has been done here. The blade flapping and pitching dynamics are evaluated with the air loads from the previous revolution of the rotor. Calculations converge within 3 to 4 coupling iterations.

5. PREVIOUSLY PUBLISHED VALIDATION OF THE HIGH-FIDELITY MODEL FOR DRY ROTOR

This section and the following section present sample results from the high-fidelity approach. It should be emphasized that these are previously published results from Ref. 9. The only purpose of our including these results in this work is to provide a comparison between the high- and low-fidelity methods.

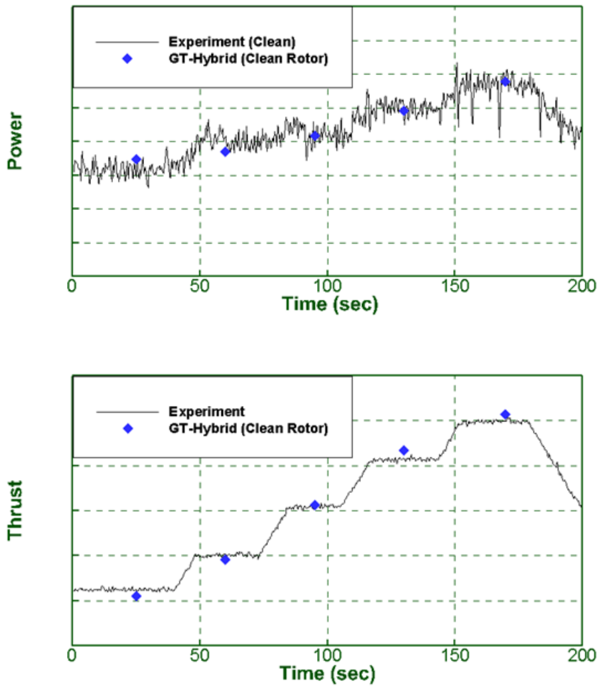

Figure 5: Computed and Measured Dry Rotor Thrust and Power (Run 84, 60 knots tunnel speed, 14° F). Results were previously published in Ref. 9.

Prior to application of the high-fidelity flow solver to icing applications, extensive work was done to validate the flow solver for dry conditions, without icing. A particular condition called Run 84, where the rotor RPM is 1200, and the tunnel freestream velocity is 60 knots has been considered. Test data is available for collective pitch angles 0°, 2°, 5°, 8°, and 10°. The tunnel was run at an ambient temperature of -10° C (14° F). The blade motion (flapping angle) is computed from a coupled CFD / Flapping Dynamics analysis of the clean rotor. Three loosely coupled iterations between the rotor dynamics solver and the hybrid CFD solver were sufficient at each collective pitch to achieve repeatable solutions. Satisfactory agreement for the rotor thrust and torque is seen in Figure 5.

6. PREVIOUSLY PUBLISHED VALIDATION OF THE HIGH-FIDELITY MODEL FOR ICE ACCRETION PHENOMENA

Sample results with the high-fidelity approach are shown in Figure 6 for the ambient conditions shown in Table 1. A multi-step time marching process is used. The ice shapes were updated once every 60 seconds of ice accretion period. The ice-shapes were computed in one of two ways – using the in-house ice accretion model, or LEWICE. Both ice accretion analyses used the same flow properties – surface pressure distribution, water droplet collection efficiency, and surface skin friction data. The predicted ice shapes are seen to be in qualitative agreement with measured shapes, although many of the irregular features seen in the measurements were not captured in the present approach.

Table 1: Test Conditions for Run53 (NASA Glenn Icing Research Tunnel)

Parameter	Value
Forward Velocity (knot)	60
RPM	1200
Collective (Deg.)	2
LWC (g/m^3)	0.5
MVD (μm)	15
Temperature (K)	263.15
Time (min)	3

The predicted thrust and power of iced rotor have also been compared with measured values (unpublished data). The computed and measured thrust values are in reasonable agreement for the dry and iced rotor both, with 16% loss in thrust attributable to icing effects. The predicted power is increased by 35% due to ice formation compared to the dry rotor. The measured power however indicates a five-fold rise relative to the dry rotor due to icing. Such a high rise in torque was not seen in other test conditions. The cause for this large discrepancy is not known at this writing.

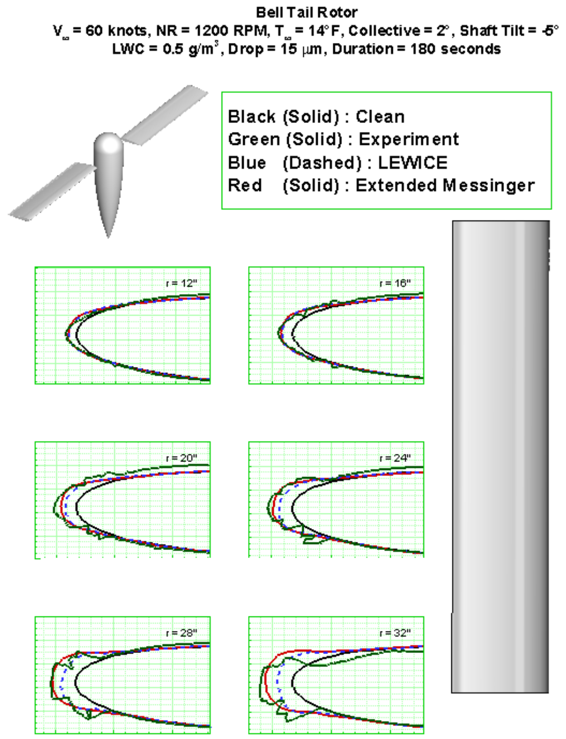

Figure 6: Computed Ice Shapes using the High-Fidelity Model for the Flow conditions Shown in Table 1. Results were previously published in Ref. 9.

7. LOW-FIDELITY MODEL FOR THE DRY ROTOR

A low fidelity model for the teetering tail rotor has also been developed, and subsequently applied for icing conditions. Calculations were done in the following order.

As a first step, the airfoil lift and load characteristics are developed. An in-house 2-D Navier-Stokes solver is used for this purpose, although other solvers such as XFOIL may be used. In the absence of such data, thin airfoil theory may be used to determine the variation of the lift coefficient as a function of angle of attack, and a nominally constant drag coefficient may be assumed.

The second order differential equations (3) and (4) were integrated in time, using a two-step Runge-Kutta scheme, starting with arbitrary initial values of zero for the flapping angle β and the flapping velocity $d\beta/dt$, with the pitching angle θ initialized to the collective pitch.

Blade element theory was used to compute the airloads. At the center of each element of chord length c, the in-plane component of velocity U_T and the component of velocity normal to the rotor disk U_P were computed. The normal component of velocity U_P at a particular blade element at a radial location r and azimuthal position ψ depends on the shaft angle of attack, freestream velocity, the instantaneous blade flapping angle and flapping velocity, and the induced inflow velocity (Based on Glauert's inflow model and thrust coefficient from the previous revolution) as shown in Figure 7.

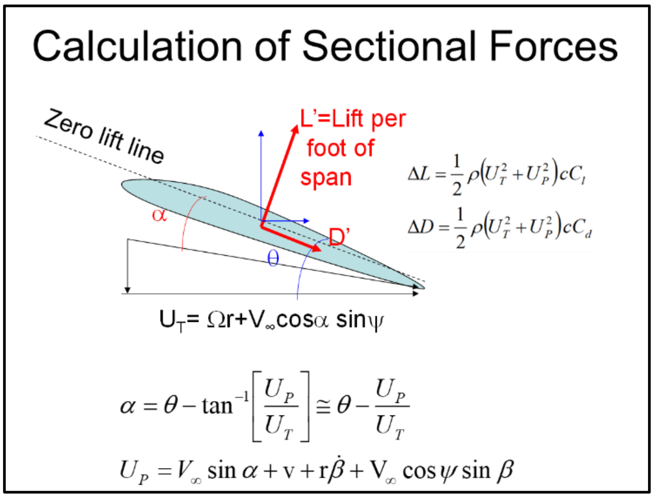

Figure 7: Procedure for Computing the Instantaneous Angle of Attack

Once the instantaneous angle of attack was known at a given blade element at any instance int time, the airfoil database was consulted to compute the quasi-steady sectional lift and drag coefficients, and this information was used to compute the lift and drag forces per unit span. The component of the force Fz normal to the plane of rotation was found, for use in equation (3). The component of force in the plane of rotation was also found and used to determine the induced power and profile power contributions from that blade element.

LOW-FIDELITY MODEL FOR THE ICED ROTOR

The iced rotor calculations relied on the dry rotor calculations and followed a very similar process. The radial variation of azimuthally averaged angle of attack was captured from the dry rotor calculations. This information, along with ambient temperature, liquid water content, and the droplet diameter were used to compute ice shapes at selected radial locations using LEWICE and an in-house ice accretion solver GT-ICE, both, The iced airfoils shapes generated using GT-ICE were reanalyzed with an in-house 2-D Navier-Stokes analysis, to obtain drag polar for the iced sections. The rotor was reanalyzed using the low-fidelity methodology, with the iced airfoil load characteristics, to recompute thrust and power.

8. INTEGRATED HUB LOADS USING THE LOW-FIDELITY MODEL FOR THE DRY ROTOR

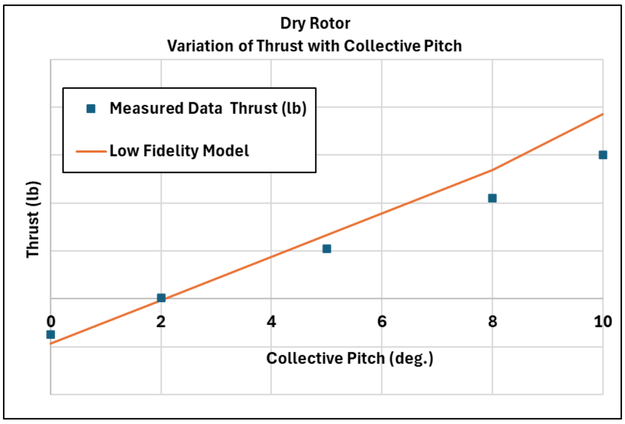

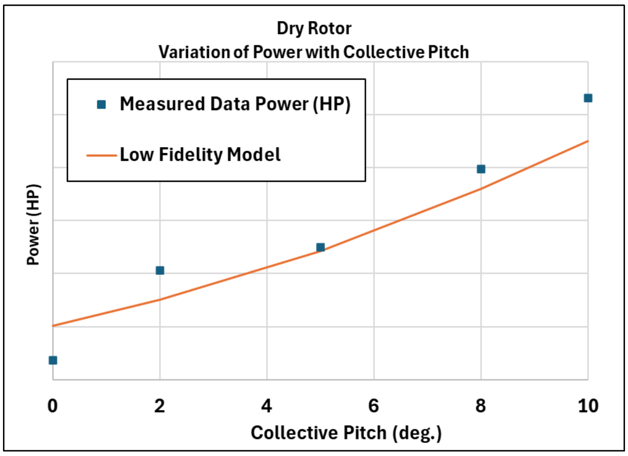

Figure 8: Variation of Thrust and Power for the Dry rotor (Run 84, 1200 RPM, 60 knots tunnel speed)

Figure 8 shows the variation of thrust and power with collective pitch for Run 84, which corresponds to a tunnel speed of 60 knots and a rotor RPM of 1200. The rotor shaft is tilted forward towards the oncoming airstream at an angle of 5 degrees. The vertical axes values are not shown in these graphs because of the proprietary nature of the data. The computed thrust values are somewhat higher by ~ 20% compared to test data, particularly at higher pitch settings, indicating that the airfoil data used in the low fidelity model may have a slightly higher lift curve slope than observed in the test data. The predicted power was also higher than the test data, with a 15% to 25% discrepancy over the range of pitch settings considered. These differences were, however, within the large scatter observed in the test data as the hub loads were collected multiple times over several hundred revolutions.

9. ICE SHAPES USING THE LOW-FIDELITY MODEL

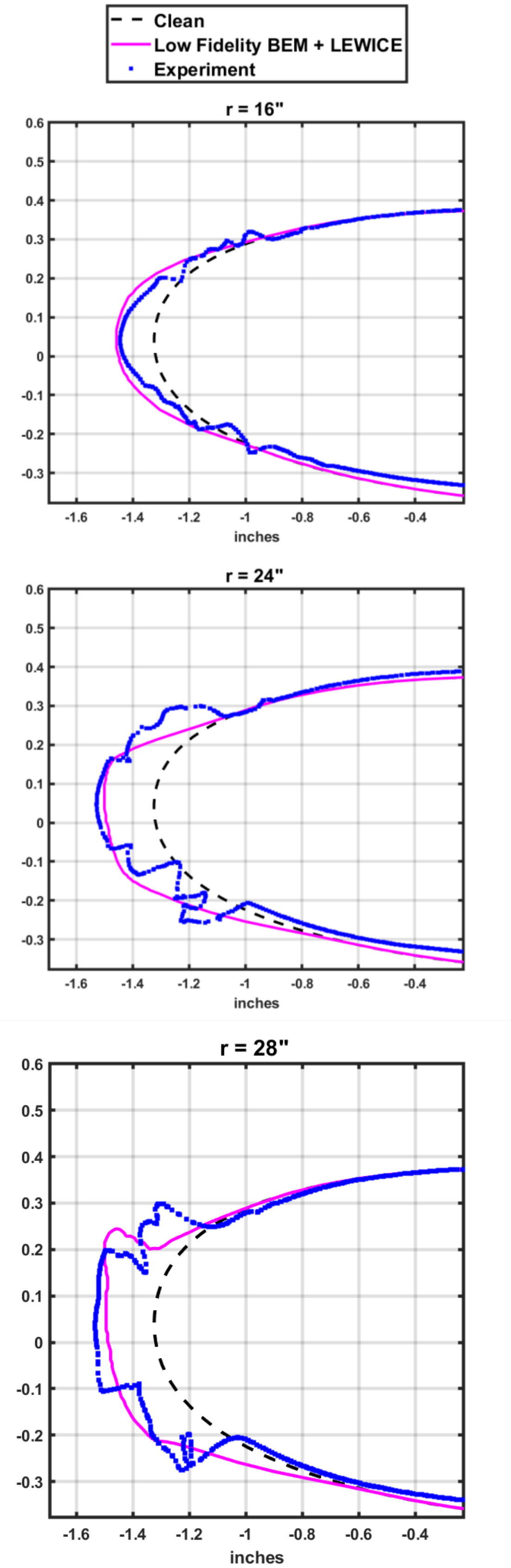

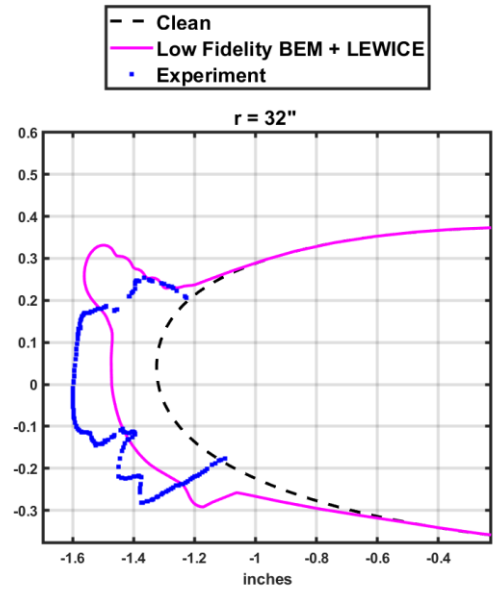

Figure 9: Ice Shapes using Low-Fidelity Approach for Run 53

Figure 9 shows the ice shapes generated using LEWICE, with the effective angles of attack computed from the low fidelity blade element method. LEWICE requires only the azimuthally averaged values of the in-plane velocity and the effective angle of attack at each radial location, in addition to ambient temperature, liquid water content, and droplet diameter for the analysis. Figure 9 shows the computed ice shapes at four radial locations - 20", 24", 28" and 32". As noted earlier, the rotor radius is 32.9". Reasonably good agreement between the computed ice shapes from these approaches is seen. The thickness of the ice in front of the blade nose and on either side of the airfoil section are captured well except near the tip.

It is of interest to see how well these predictions compare with the high-fidelity simulations shown in Figure 6, and the ice shape predictions computed using the in-house solver GT-ICE. Figure 10 shows the comparisons from these approaches. The high-fidelity approaches predicted the thickness of the ice in front of the nose and sides of the airfoil, However, the Eulerian approach used in the flow solver (GT-Hybrid), the droplet transport solver (GT-DROP), and the ice accretion solver (GT-ICE) generated a smooth ice shape, and many of the finer details of the ice shape were not captured. A much finer grid in the leading-edge region, combined with an unstructured grid-based flow and ice accretion analysis, may be needed to resolve and capture the finer details of the ice shape.

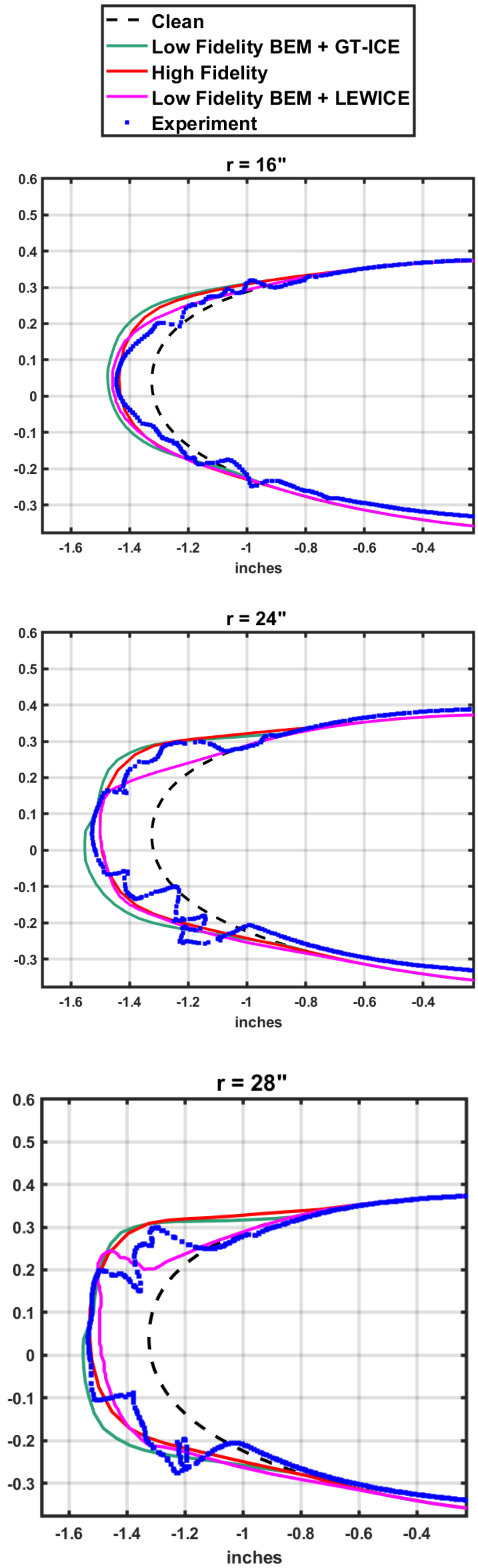

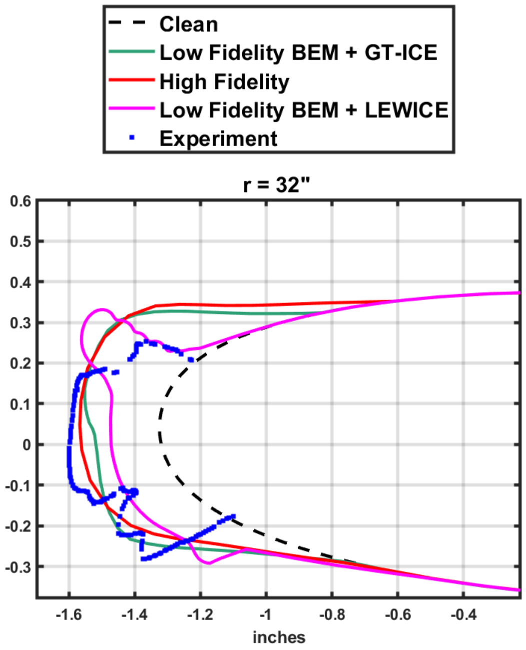

Figure 10: Comparison Ice Shapes using Low- and High-Fidelity Approach for Run 53

10. INTEGRATED HUB LOADS USING THE LOW- AND HIGH-FIDELITY MODEL FOR THE ICED ROTOR

Table 2 shows the comparisons between the low- and high-fidelity tools described in this work, and test data. The low fidelity simulation was trimmed to a slightly lower collective pitch of 1.85 degrees to match the computed thrust to the predictions with the high-fidelity flow solver, GT-Hybrid.

Table 2: Low and High Fidelity comparisons with measured data for Run 53 at 1200 RPM, T = 14 F, V=60 knots.

	Thrust (lb)	Power (HP)
Measured Dry	-2.53	0.5
Measured Iced	-2	3.5*
GT-Hybrid Dry	-1.86	0.75
GT-Hybrid Iced	-1.69	1.01
Low-Fidelity, Dry, 1.85 deg pitch	-1.95	0.735
Low-Fidelity, Iced, 1.85 deg pitch	-2	0.874

When the rotors are trimmed to the same thrust setting, the low and high-fidelity cases for the dry rotor predict power values that are within 2% of each other. Icing had a negligible effect on thrust for this specific case, approximately 0.17 lb for GT-Hybrid and 0.05 lb for the low fidelity case. GT-Hybrid predicted a power rise of 0.26 HP ~35% increase) while the low fidelity model predicted a power rise of 16% for the iced rotor relative to dry rotor.

Comparisons with test data may also be made. The measured thrust is within 0.5 lb of low and high-fidelity simulations both.

The test data, however, shows a five-fold increase in power for the iced rotor. Such a sharp rise in power was not seen in data at other test conditions and could not be explained given the small changes to the profile of computed and measured rime ice accretion.

11. SUMMARY AND CONCLUSIONS

A low-fidelity model has been developed for modeling two-bladed teetering rotors, with pitch-flap coupling. This rotor has been analyzed under dry and icing conditions, both. The ice shapes are computed using low cost 2-D ice accretion models such as LEWICE or GT-ICE, allowing the overall simulation time to be low. All the simulations may be done on a desktop computer system in a matter of minutes.

Comparisons of the hub loads with test data have been made for the dry rotor, and the iced rotor for a specific condition shown in Table 1. Ice shapes have also been computed. At this writing, the agreement with test data is qualitative for the ice shapes and hub loads both. The low fidelity tool developed here, in its present form, is suitable primarily for quickly analyzing various icing conditions (liquid water content, droplet diameter distribution, ambient temperature, tip speed, forward speed, rotor RPM), to qualitatively assess the impact of icing on the loss of thrust and rise in power.

Author contact:

Aishwerya Gahlot aishwerya@gatech.edu

Jeewoong Kim jeewoong.kim@lmco.com

Lakshmi N. Sankar lsankar@ae.gatech.edu

12. ACKNOWLEDGEMENTS

This research was partially funded through the U.S. Army/Navy/NASA Vertical Lift Research Center of Excellence at Georgia Tech under the direction of

Mahendra Bhagwat of the US Army Futures Comment, Agreement No. W911W6-21-2-0001. Opinions, interpretations, conclusions, and recommendations are those of the authors and are not necessarily endorsed by the United States Government. This research was supported in part through research cyberinfrastructure resources and services provided by the Partnership for an Advanced Computing Environment (PACE) at the Georgia Institute of Technology, Atlanta, Georgia, USA.

13. REFERENCES

1. Potapczuk, M. G., and Reinmann, J. J., "Icing Simulation: A Survey of Computer Models and Experimental Facilities," AGARD, Effects of Adverse Weather on Aerodynamics, 1991.

2. Bourgault, Y., Boutanios, Z., and Habashi, W. G., "Three-Dimensional Eulerian Approaches to Droplet Impingement Simulations Using FENSAP-ICE, Part 1: Model, Algorithm, and Validation," Journal of Aircraft, Vol. 37 No.1, 2000.

3. Wright, W. B., "LEWICE 2.2 Capabilities and Thermal Validation," AIAA Paper 2002-0383, 2002.

4. Habashi, W. G.," Recent Advances in CFD for In-Flight Icing Simulation," Japan Society of Fluid Mechanics, Vol. 28, No. 2, 2009,pp. 99-118.

5. Narducci, R. and Kreeger, R., "Analysis of a Hovering Rotor in Icing Conditions," Proceedings of American Helicopter Society 66th Annual Forum, 2010.

6. Narducci, R., Orr, S. and Kreeger, R., "Application of a High-Fidelity Icing Analysis Method to a Model-Scale Rotor in Forward Flight," Proceedings of American Helicopter Society 67th Annual Forum, 2011.

7. Kreeger, R. E. And Tsao, J., "Ice Shapes on a Tail rotor," AIAA Paper 2014-2612, 6th AIAA Atmospheric and Space Environments Conference, Atlanta, GA, June 2014.

8. Wright, J., Aubert, R., "Icing Wind Tunnel Test of a Full-Scale Heated Tail Rotor Model," American Helicopter Society 71st Annual Forum, Virginia Beach, Virginia, May 5-7, 2015.

9. Kim, Jeewoong, "Development of a Physics Based Methodology for the Prediction of Rotor Blade Ice Formation," PhD Dissertation, Georgia Institute of Technology, December 2015.

10. Kreeger, R. E., Sankar, L. N., Nucci, M., and Kunz, R., "Progress in Rotorcraft Icing Computational Tool Development," SAE Technical Paper 2015-01-2088, 2015, doi:10.4271/2015-01-2088.

11. Messinger, B. L., "Equilibrium temperature on an unheated icing surface as a function of airspeed," J. Aeronautical Sci. Vol. 20, 1953, pp. 29-41.

12. Gahlot, A., Sankar, L. N., and Chen, Po-Wei, "Effects of Light Rain on Coaxial and Tandem Rotors in Hover," Proceedings of the Vertical Flight Society Annual Forum, May 2023.